First Principles Insight of Structural, Vibrational, Mechanical and Optoelectronic Properties of LiBH4 for Hydrogen Storage and Optoelectronic Devices

R. M. Arif Khalil[1], Muhammad Iqbal Hussain[1], Fayyaz Hussain[1], A. Manzoor Rana[1,1], G. Murtaza[2], Muhammad Shakeel[1], and Muhammad Imran[3]

[1]Bahauddin Zakariya University
[2]Government College University Lahore
[3]Government College University Faisalabad

June 1, 2020

Abstract

To cope with the energy crisis and global warming issues, researcher are rendering their efforts and paying their attentions to analyze and fabricate hydrogen storage devices. In this regard, we report a comprehensive study on the structural, vibrational, and optoelectronic properties of Lithium Borohydride (LiBH4), a hydrogen storage material. For this purpose, calculations of structural properties have been made using the local, non-local and hybrid functionals within the framework of density functional theory (DFT). The lattice constants for the orthorhombic phase are determined by applying LDA, PBE and HSE06 density functionals and their results are compared with available experimental and theoretical studies. In order to determine IR and Raman active modes of vibrations, vibrational spectroscopy has been utilized through Density Functional Perturbation Theory (DFPT) approach. Li, B and H atoms are noticed to be contributing in the modes of vibrations between different ranges of frequencies, i.e., 0 to 400 cm-1, 1100 to 1300 cm-1 and 2250 -2400 cm-1. The respective values of band gaps are found to be 6.35 eV, 6.81 eV and 7.58 eV for LDA, PBE and HSE06 functionals, respectively, leading to indicate insulating nature of LiBH4 which makes it a promising candidate for applications in optoelectronic devices. The mechanical analysis reveals that LiBH4 is a brittle material. The optical properties such as dielectric constant, refractive index, reflectivity, absorptivity, conductivity and loss function are also calculated with the aid of well-recognized relation of Kramer-Kronig. The plasma frequency is noted at the highest peak (13.7 eV) of the energy loss function.

Abstract:

To cope with the energy crisis and global warming issues, researcher are rendering their efforts and paying their attentions to analyze and fabricate hydrogen storage devices. In this regard, we report a comprehensive study on the structural, vibrational, and optoelectronic properties of Lithium Borohydride ($LiBH_4$), a hydrogen storage material. For this purpose, calculations of structural properties have been made using the local, non-local and hybrid functionals within the framework of density functional theory (DFT). The lattice constants for the orthorhombic phase are determined by applying LDA, PBE and HSE06 density functionals and their results are compared with available experimental and theoretical studies. In order to determine IR and Raman active modes of vibrations, vibrational spectroscopy has been utilized through Density Functional Perturbation Theory (DFPT) approach. Li, B and H atoms are noticed to be contributing in the modes of vibrations between different ranges of frequencies, i.e., 0 to 400 cm^{-1}, 1100 to 1300 cm^{-1} and 2250 -2400 cm^{-1}. The respective values of band gaps are found to be 6.35 eV, 6.81 eV and 7.58 eV for LDA, PBE and HSE06 functionals, respectively, leading to indicate insulating nature of $LiBH_4$ which makes it a promising candidate for applications in optoelectronic devices. The mechanical analysis reveals that

LiBH4 is a brittle material. The optical properties such as dielectric constant, refractive index, reflectivity, absorptivity, conductivity and loss function are also calculated with the aid of well-recognized relation of Kramer-Kronig. The plasma frequency is noted at the highest peak (13.7 eV) of the energy loss function.

Keywords : optoelectronic devices, hydrogen storage, vibrational spectroscopy, IR and Raman modes, electronic band gap, loss function.

Introduction

Over the next 30 years, two major challenges would be facing by this era of the Science and Technology: (a) curtailing supply of the fossil fuels and (b) destructive impact of the growth rate of global warming on the climate changes. That is why, researchers of the day are being motivated to render their optimal efforts and paying their full attentions to manufacture hydrogen storage devices [1-2]. The bountiful amount of natural water, available in the universe, is a fundamental and inexhaustible source of hydrogen which could be utilized as an alternative and renewable source of energy. Nonetheless, it has been a vital challenge for the researchers as well as industrial community of the current era to mystified, predict and explore novel combinations of materials which is ought to be advantageous in devising such an appropriate device wherein hydrogen could be stored more efficiently and largely for its mobile applications [3-4]. Among various capable hydrogen storage materials, $LiBH_4$ is one to be considered for such hydrogen storage devices. This material was studied by Wang *et al.* [5] to examine the phase transitions occurring at pressures of 1.64 GPa and 2.83 GPa along with its electronic properties through the first principles approach. Setten *et al.*[6] have reported that the optical response of the simple and complex hydrides is found to be similar, despite the fact that their electronic band gaps are of different values. Xiaohua *et al.*[7] have investigated the dehydrogen characteristics of $LiBH_4$ modified by Mg and showed that Mg can destabilize $LiBH_4$ by reducing the energy cost required for H-desorption. Miwa *et al.* [8] studied its structural, electronic, vibrational and heat of formation along with its vibrational modes of vibrations. Ikeshoji *et al.* [9] reported the ionic conductivity of Li^+ ions in $LiBH_4$system, wherein, activation energy and diffusion coefficient were estimated by vesting theoretical as well as experimental studies. Song*et al.* [10] have studied the metal borohydride ammonia borane complex using $LiBH_4$ and NH_3BH_3. They found both of these systems to be thermodynamically stable. Benzidi *et al.* [11] have compared the vibrational and thermodynamical properties of $LiBH_4$ in orthorhombic and hexagonal phases, wherein, they reported that orthorhombic phase of $LiBH_4$ is more stable thermodynamically. Khalil *et al.* [12] recently studied the spectroscopic and thermodynamical properties of a similar hydride, MgH_2 in the presence of catalysts and found that hydrogen release temperature is reduced due to reaction of metal hydride with catalysts. Ghellab *et al.* [13] reported the phase transition in $LiBH_4$ system at high values of pressure based on density functional theory calculations using the WIEN2K code.

Although few studies display the vibrational and optical behavior of $LiBH_4$, nevertheless, for better insights into it, the critique on various modes of vibrations and optical response of $LiBH_4$ through CASTEP simulation code is still unaddressed. Therefore, we are motivated to study this imperative compound by utilizing various local, non-local and hybrid functionals for better and improved electronic properties as well as insight into the vibrational characteristics. The results are discussed and compared for their suitability in utilizing them for the hydrogen storage and other optoelectronic applications.

Research Methodology

All calculations are carried out using density functional theory as implemented in CASTEP simulation code [14]. The norm-conserving pseudopotentials [15-17] have been used to model electron-ion interaction along with plane-wave cut-off energy of 884 eV to converge the $LiBH_4$ system in order to attain the structural properties. The Monck-Pack [18] grid of the values of $8\times4\times8$ was selected to sample the Brillouin zone. The conjugate gradient method [19] was selected to relax the ionic positions, cell volume and lattice parameters of the systems until the Hellmann Feynman forces [20] found smaller than 0.02 eV/Å and the energy convergence criteria was met at 10 μeV. The most popular functionals LDA, GGA-PBE and HSE06 [21-23] are used to apply exchange correlation potentials in solving the Kohn-Sham [24-25] equations for the structural and electronic properties. The vibrational properties are calculated using the density functional perturbation

theory [26]. Kramer-Kronig [27-28] relations have been adopted to determine the optical properties of $LiBH_4$. The GGA-PBE functional was adopted for determining vibrational and optical properties.

1. **Results and Discussion**
2. **Structural Properties**

The geometrically optimized crystal structure of a unit cell of $LiBH_4$ is shown in figure 1. Red color balls represent lithium atoms, green color ones indicate boron atoms and blue color ones define hydrogen atoms. There are a total of 24 atoms in a primitive unit cell of $LiBH_4$, which are further split into 16 hydrogen atoms, 4 lithium atoms and 4 atoms of boron as obvious from figure 1.

The optimized cell angles and lattice constants determined through CASTEP code are summarized in the table-1. It is noticeable that present outcomes regarding cell angles and lattice constants obtained through GGA-PBE functional are found to be in more-closer agreement with the former experimental results [29] as compared to these determined through LDA and HSE06 functionals (see Table-1). The highest deviation in lattice constants is noted for HSE06 functionals, which is underestimating the values of lattice constants for $LiBH_4$ system.

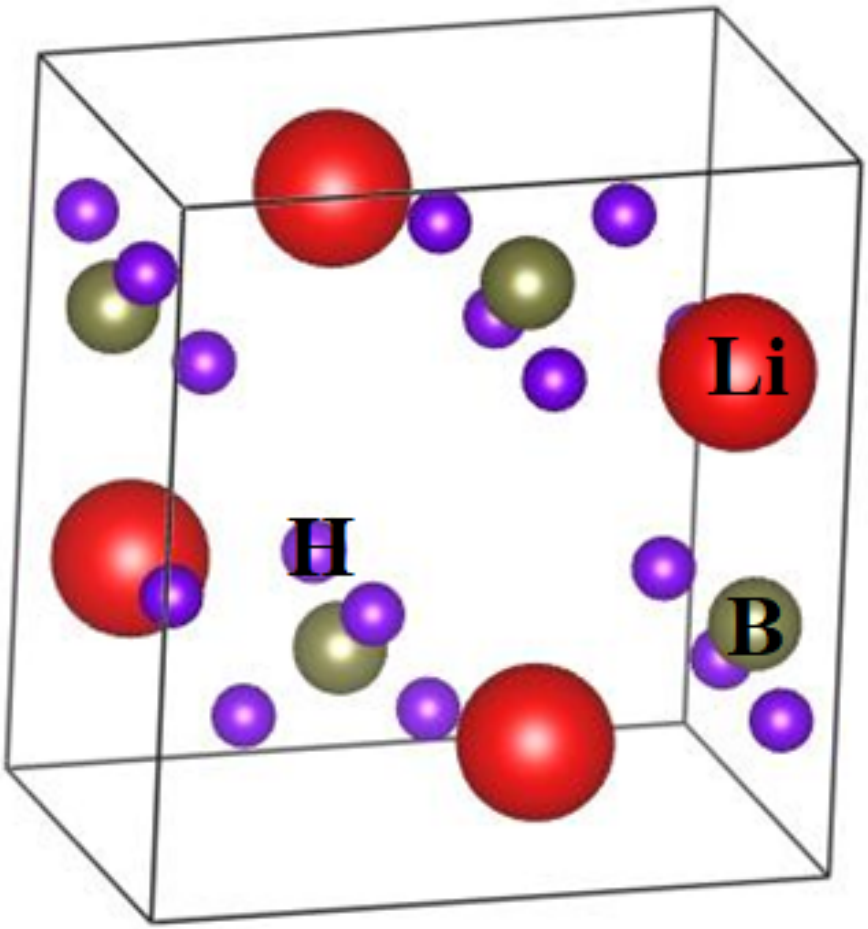

Figure 1: Optimized crystal structure of $LiBH_4$.

Table-1: Lattice parameters and cell angles of $LiBH_4$.

Material	Approach	Lattice constant (Å)	Lattice constant (Å)	Lattice constant (Å)	Cell angle (degree)	Cell angle (degree)	Cell angle (degree)
$LiBH_4$	**Functionals**	**a**	**b**	**c**	**α**	**β**	**γ**
	LDA [Present Study]	6.947	4.251	6.471	90°	90°	90°
	PBE [Present Study]	7,146	4.387	6.642	90°	90°	90°
	HSE06 [Present Study]	6.276	4.115	6.241	90°	90°	90°
	Experimental Results [29]	7.137	4.417	6.703	90°	90°	90°

Vibrational Properties

The frequency vs phonon dispersion curves, and frequency vs density of states plots for the considered compound are shown beside each other in figure 2, wherein, the modes of vibrations are found to exist in the frequency range of 0 to 2500 cm^{-1} between the symmetry points G and Z of the first Brillouin zone. Figure 2 (a) depicts that there are no imaginary frequencies (soft modes) seen at gamma symmetry G. It is noteworthy that out of the possible 72 modes of vibrations, three belong to acoustic branches and remaining 69 modes of vibrations are associated with optical branches. The vibrational states seen in the frequency range of 0 to 400 cm^{-1} have been occurred due to the contribution of displacement of $Li^+$and $[BH_4]^-$ ions. While, the vibrational states in the frequency range of 1050 to 1300 cm^{-1} are present due to contribution of B and H atoms. Finally, the H atom having least atomic mass portrays vibrational states in the frequency range 2300 to 2400 cm^{-1}. Moreover, as shown in figure 2 (b) 1^{st} dominant peak of density of state noted at a frequency of 250 cm^{-1} might belong to the displacements of $Li^+$and $[BH_4]^-$ ions. Likewise, 2nd dominant peak (the highest peak) appeared at frequency of about 1000 cm^{-1}, which is ought to become available due to the influence of B and H atoms. And that the third important peak, which is recognized as 2^{nd} highest peak, noticed at frequency of about 2300 cm^{-1} might have appeared due to partaking of H atoms.

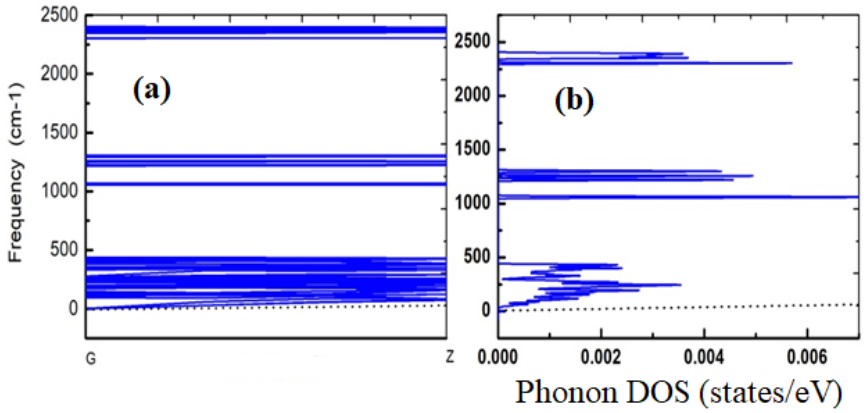

Figure 2: The calculated plots for (a) frequency vs phonon dispersion curves (b) frequency vs density of states.

Infrared and Raman Spectroscopy

We have used Density Functional Perturbation theory [30] in order to revealthe Infrared (IR) and Raman spectroscopy. IR and Raman modes of vibrations obtained for the studied compound are displayed in table 2. As shown in figures (3-4), modes at values of frequency 93.224 cm^{-1}, 113.244 cm^{-1}, 251.0 cm^{-1} and 436.144 cm^{-1} are observed due to displacement of $Li^{+}$and $[BH_4]^{-}$ ions. At the values of frequency of 1054.1 cm^{-1} and 1305.3 cm^{-1}, bending modes of vibration occurred due to H and B atoms. The symmetrical modes of vibration have been observed at the values of 2303.5 cm^{-1}, 2387.5 $cm^{-1}$and 2401.6 cm^{-1}, whereas, antisymmetrical modes of vibration were observed at frequencies of 2345.920 cm^{-1} and 2377.9 cm^{-1} due to motion of H atoms. Our calculated Raman active and IR active modes are found to be consistent with the available experimental studies [45]. The calculated modes of vibrations are in close agreement with the earlier theoretical studies with some slightly different modes [31]. The possible reason may be the use of different calculation approaches and the terms related to interactions and exchange potentials etc.

Table 2: Infrared and Raman spectroscopy of $LiBH_4$. Character of modes are represented as inactive (i), Raman active (R), and infrared active (IR) and irreducible representation (Irrep.).

Frequency (cm^{-1})	**Irrep.**	**Character of Modes**	**Modes of Vibrations**
93.2	Au	i	displacement of Li^{+} and $[BH_4]^{-}$ ions
113.2	B1g	R	displacement of Li^{+} and $[BH_4]^{-}$ ions
147.2	B1u	IR	displacement of Li^{+} and $[BH_4]^{-}$ ions
172.2	B3g	R	displacement of Li^{+} and $[BH_4]^{-}$ ions
195.2	B2u	IR	displacement of Li^{+} and $[BH_4]^{-}$ ions
246.2	B3u	IR	displacement of Li^{+} and $[BH_4]^{-}$ ions
251.1	B1u	IR	displacement of Li^{+} and $[BH_4]^{-}$ ions
436.1	B1g	R	displacement of Li^{+} and $[BH_4]^{-}$ ions
1054.1	Au	IR	Bending
1068.6	B2g	R	Bending
1217.2	Ag	R	Bending
1249.1	Au	IR	Bending
1294.1	B3u	IR	Bending
1303.2	B2g	R	Bending
1305.3	Ag	R	Bending
2303.5	Ag	R	Symmetrical Stretching
2305.2	B3u	IR	Symmetrical Stretching
2345.9	Ag	R	Asymmetrical Stretching
2377.7	B1u	IR	Asymmetrical Stretching
2384.6	B3u	IR	Symmetrical Stretching
2387.5	Ag	R	Symmetrical Stretching
2401.6	B2g	R	Symmetrical stretching

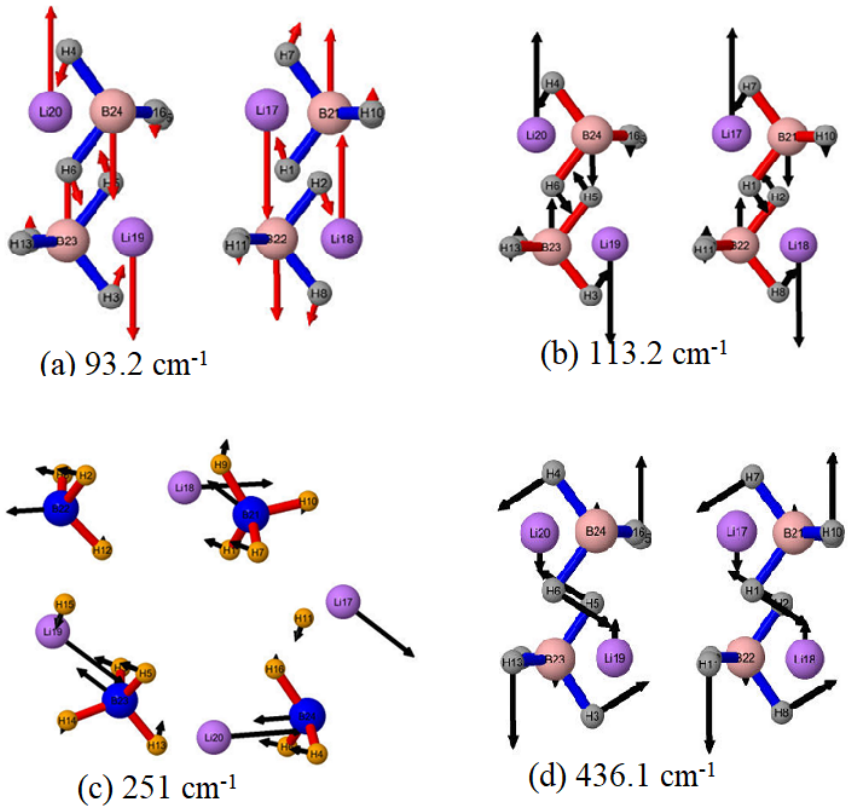

Figure 3: At different frequencies, the displacement ofLi^+ and $[BH_4]^-$ ions.

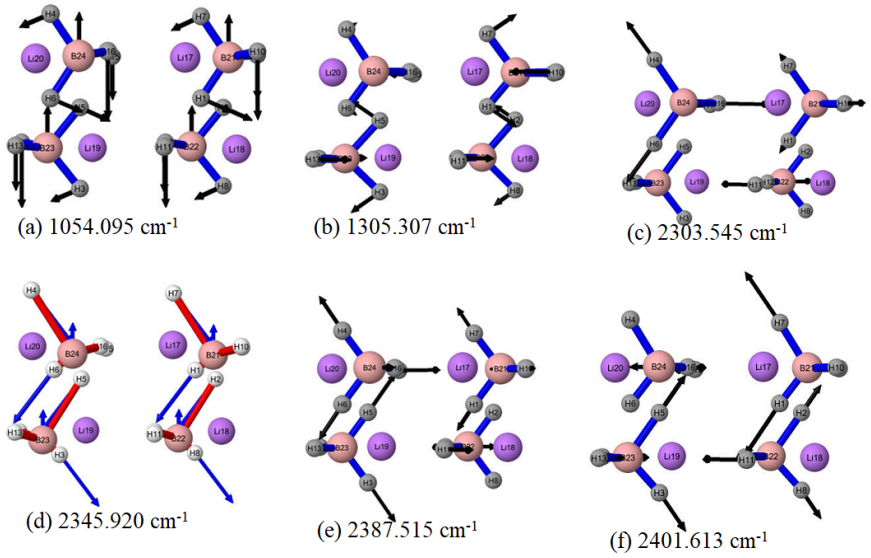

Figure 4: Various modes of vibration at different frequencies: (a-b) bending, (c) symmetrical stretching, (d) asymmetrical stretching, (e-f) symmetrical stretching.

Electronic Properties

The electronic structure calculations have been carried out using CASTEP simulation code. The electronic density of states and band structure shown in figures (5-7) are calculated by utilizing LDA, PBE and HSE06 functionals, respectively. Figures (a) reveal band structures while figures (b) demonstrate corresponding DOS plots. In all figures (5-7) (a), it has been noticed that the electron-hole pair recombination took place at Γ (gamma) symmetry point of the first Brillouin Zone with a significant energy gap of magnitudes 6.35 eV, 6.81 eV and 7.58 eV using LDA, PBE and HSE06 functionals respectively, leading to the direct band gap insulating material. As depicted by the figure (5-7) (b), the density of states are found in wide range of energy, i.e., from 13.96 eV to -7.5 eV, 9.51 eV to -7.5 eV, and 15 eV to -7.5 eV for respective functionals. The highest edge of the valence band (VBM) is found on the Fermi level, which is set at zero energy, while lowest edges of the conduction bands (CBM) are noted at 6.35 eV, 6.81 eV and 7.58 eV for three different functionals, i.e., LDA, PBE and HSE06 respectively. 1s, $1s^2$ $2s^1$, and $2s^2 2p^1$ are the pseudo-states for H, Li, and B atoms respectively which are contributing in conduction mechanism. The highest value of band gap for HSE06 functional is due to underestimating the lattice constants as mentioned in structural properties section 3.1. Comparatively, it has been concluded that our theoretically estimated value of the band gap of 6.81 eV using PBE functional is ˜4.1% smaller than the former experimental value of 7.1 eV reported for $LiBH_4$ [27], which is an acceptable precision range. The value of band gap was found to be very close to the previously reported values of 6.80 eV and 6.95 eV by Miwa *et al.*and Ghellab *et al.* [31-32] respectively using diverse calculation codes. Figure 8 illustrates the behavior of atomic orbitals of each element of the studied compound. From this figure, it is seen that in the conduction band region, *p* -states of Li atoms mainly contribute between the energy range 7.0 eV to 12.5 eV. However, denser bands near the Fermi level and large peaks in density of states are seen due to *p* -state of B atoms and *s* -states of H atoms in energy range from -2.5 eV to 0 eV in the valence band. The*s* -states of H and B atoms lie in lower region of the valence bands in between -7.5 eV to -5.2 eV energy range which look exactly similar to total density of states in this region of valence band.

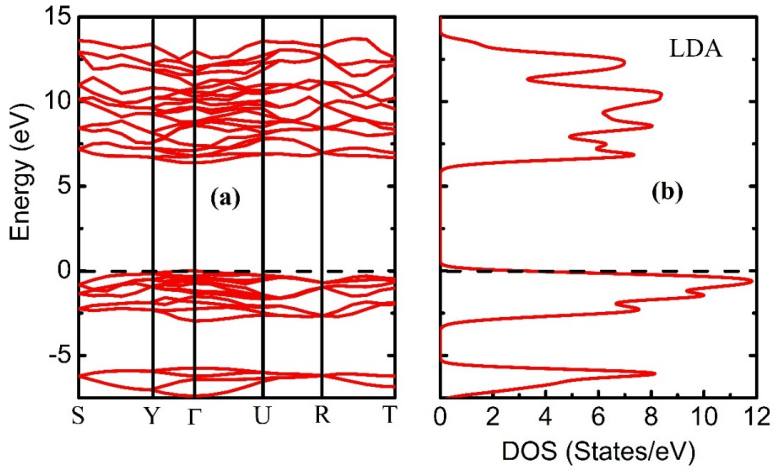

Figure 5: Calculated (a) band structure (b) electronic density of states using LDA functional.

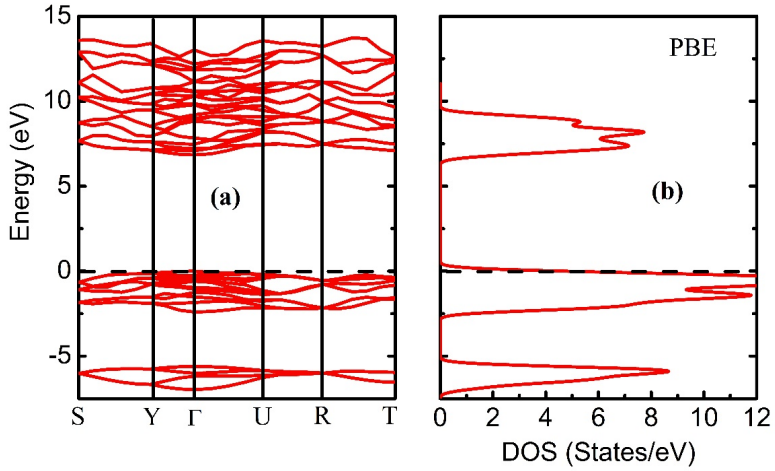

Figure 6: Calculated (a) band structure (b) electronic density of states using PBE functional

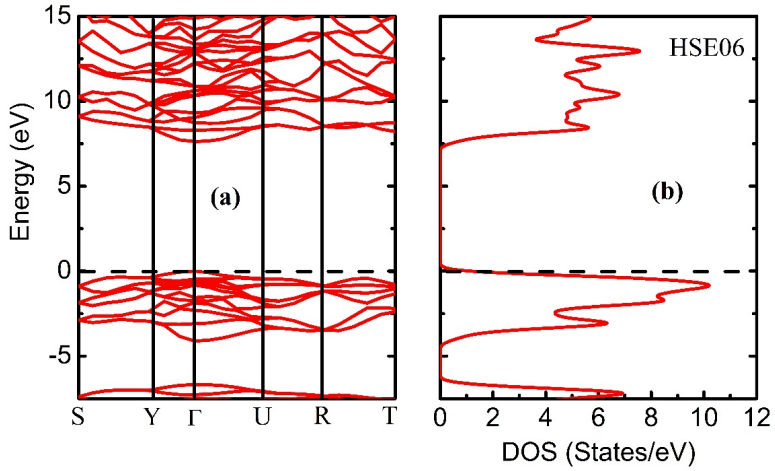

Figure 7: Calculated (a) band structure (b) electronic density of states using HSE06 functional

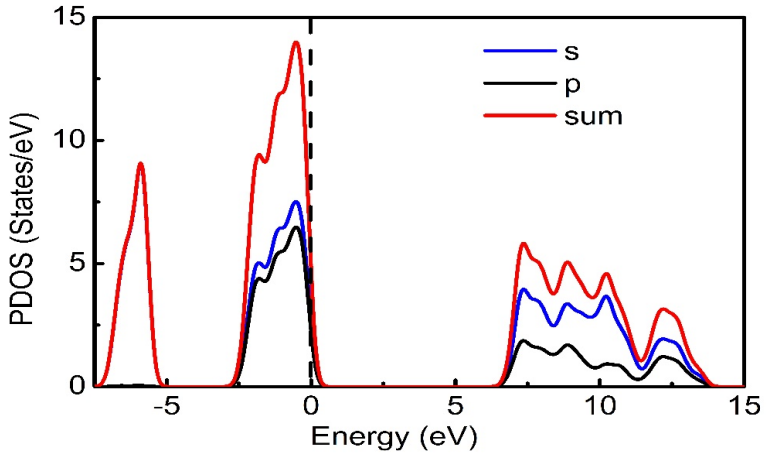

Figure 8: Calculated projected density of states using PBE functional

Mechanical properties

For $LiBH_4$ with the orthorhombic crystal structure, there are nine independent-elastic-constants namely C_{11}, C_{12}, C_{13}, C_{22}, C_{23}, C_{33}, C_{44}, C_{55}, and C_{66}. They should satisfy the following Born's stability criterions [33] for mechanical stability which is found to be satisfied rigorously according to our outcomes as given in table-3.

$C_{11} > 0$, $C_{22} > 0$, $C_{33} > 0$, $C_{44} > 0$,$C_{55} > 0$, $C_{66} > 0$ (1)

$[C_{11} + C_{22} + C_{33} + 2C_{12}+2C_{13} + 2C_{23}] > 0$ (2)

$C_{11} + C_{22} - 2C_{12} > 0$,$C_{11} + C_{33} - 2C_{13} > 0$,$C_{22} + C_{33} - 2C_{23} > 0$ (3)

Moreover, other mechanical parameters are calculated using Voigt-Reuss-Hill's approximation [34-35]. It is well-known that elastic properties are closely related to the basic solid state properties such as Bulk, Young and Shear moduli, thermal expansion, Debye temperature etc. The values of elastic parameters are summarized under table-3. It is worth mentioning that neither theoretical nor former experimental data is available to compare with our outcomes. Thus, mechanical behavior of the studied compound is being explored for the first time with varying pressure prior to report its fitness for hydrogen storage devices.

$$B_V = \frac{[C_{11} + C_{22} + C_{33} + 2(C_{12}+C_{13} + C_{23})]}{9} \quad (1)$$

$$B_R = \begin{array}{c}[C_{11}(C_{22} + C_{33} - 2C_{23}) + C_{22}(C_{33} - 2C_{13}) - 2C_{33}C_{12} \\ + C_{12}(2C_{33} - C_{12}) + C_{13}(2C_{12} - C_{13}) + C_{23}(2C_{13} - C_{23})]^{-1}\end{array} \quad (2)$$

Where B is Hill's bulk modulus which is average of Voigt-Reuss bulk modulus and

$$B = [B_V + B_R]/2 \quad (3)$$

$$\text{And}= C_{13}\left(C_{12}C_{23}-C_{13}C_{22}\right)+C_{23}\left(C_{12}C_{13}-C_{23}C_{11}\right)+C_{33}\left(C_{11}C_{22}-C_{12}^{2}\right) \quad (4)$$

$$G_V = \frac{[C_{11}+\ C_{22}+C_{33}+3(C_{44}+C_{55}+C_{66})-(C_{12}+C_{13}+C_{23}]}{15} \quad (5)$$

$$G_R = \begin{array}{c} 15\{4[C_{11}\left(C_{22}+C_{33}+C_{23}\right)+C_{22}\left(C_{33}+C_{13}\right)+C_{33}C_{12} \\ -C_{12}\left(C_{23}+C_{12}\right)-C_{13}\left(C_{12}+C_{13}\right)-C_{23}\left(C_{13}+C_{23}\right)]/ \\ +3[\left(\frac{1}{C_{44}}\right)+\left(\frac{1}{C_{55}}\right)+\left(\frac{1}{C_{66}}\right)\}^{-1} \end{array} \quad (6)$$

$$G = \ [G_V+G_R]/2 \quad (7)$$

Hill's Shear modulus G (GPa) is an average of Voigt-Reuss shear moduli. While the ratio of Hill's bulk and shear moduli be recognized as Pugh's ratio which is an essential parameter to predict whether the studied material associates to brittle or ductile nature [36].

Table 3: Values of the elastic constants C_{11}, C_{12}, C_{13}, C_{22}, C_{23}, C_{33}, C_{44}, C_{55}, and C_{66} in (GPa), Bulk, Young and Shear moduli in (GPa), Poisson's coefficient ν, Anisotropy factor A and Pugh's ratio $\frac{B}{G}$.

Parameter	$LiBH_4$ at 0GPa	$LiBH_4$ at 5GPa	$LiBH_4$ at 10GPa
C_{11}	37.6475	37.7028	37.6801
C_{12}	4.0323	4.0620	4.0225
C_{13}	1.7055	1.7350	1.7165
C_{22}	43.0892	43.1389	43.0551
C_{23}	2.9579	2.9457	2.9465
C_{33}	40.0196	39.9851	40.0621
C_{44}	20.6164	20.6304	20.6066
C_{55}	19.3899	19.3728	19.4046
C_{66}	19.3783	19.3936	19.3555
B	15.3120	15.3303	15.3153
Y	37.2189	37.2669	37.2522
G	19.3200	19.3239	19.3203
ν	0.0911	0.0917	0.0910
A	0.0192	0.0192	0.0188
$\frac{B}{G}$	0.7925	0.7933	0.7927

The value of Bulk modulus is not very large (15.3120 GPa), which is less than standard value of 40 GPa to specify any material a superhard [37]. While value of Young's modulus (37.2189 GPa) specifies that $LiBH_4$ is a stiffer compound. If value of the Pugh's criteria [36] $\frac{B}{G}$ >1.75 the material is said to be ductile else brittle. In our case $\frac{B}{G}$ is less than 1.75, thereby, declaring $LiBH_4$ a brittle material. Moreover, if $\nu < 0.26$ the material is deemed brittle else ductile [38], which is less than 0.26 for $LiBH_4$so it endorses its brittleness. If the value of an anisotropic factor (A) is equal to unity, the material is isotropic else anisotropic [39-40]. In our case, the value of anisotropic factor is less than unity for $LiBH_4$ which indicates its anisotropic behavior.

1. **Optical Properties**
2. **Dielectric function**

Dielectric function is deemed to be an important parameter, which is capable of illustrating the polarizability and energy loss function of any material. Particularly, its real part describes polarization of the materials, since dielectric function can be split into two parts; the real and imaginary parts which are drawn as a

function of frequency and shown in figure 9. The complex dielectric function can be expressed through well-recognized Kramer-Kronig [32-41] relation as given below:

$E(\omega) = E_1(\omega) + i\ E_2(\omega)$ (1)

Other than the dielectric function, we have also investigated frequency dependent energy loss function, refractive index, optical conductivity and reflectivity. Dielectric response of the material is mainly associated with the multiferroicity [42]. Penn's model can be expressed as [43]:

$\varepsilon_1(0) = 1 + \left(\hbar\frac{\omega_p}{E_g}\right)^2$ (2)

In this relation E_g is energy gap and ω_p is the plasma frequency.

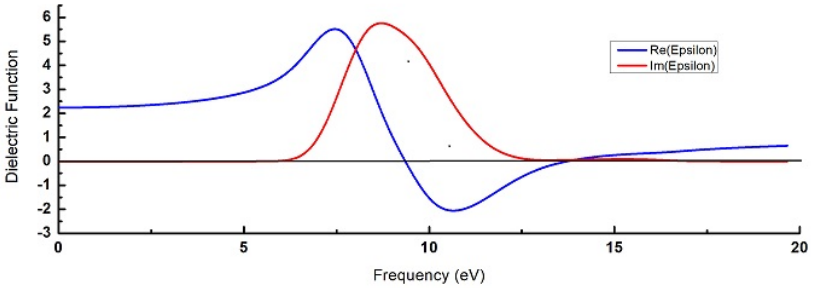

Figure 9: The calculated real and imaginary parts of the dielectric function for $LiBH_4$

In figure (9) blue line indicates the real part, while red line shows imaginary part of dielectric function. The static value of the real part of the dielectric function at zero frequency is found to be 2.25. It extends slightly along the frequency axis upto 5 eV, however, beyond this frequency, its value ascends at the higher frequency and gains maximum value of 5.6. Nevertheless, on increasing the frequency above 7.5 eV, ε_1 descends to zero at 9 eV, it further extends towards its negative values and gains the value of -2 at 10.5 eV frequency. On escalation of the frequency range above 10.5 eV, real part of dielectric function regains its value. After crossing the frequency axis at 14 eV, it extends with positive values but almost parallel to the frequency axis. Moreover, as revealed from figure (9),ε_2 the imaginary value of the dielectric function remains zero upto an energy (frequency) approximately equal to the energy band of the studied material. However, beyond 6.88 eV frequencies, the value of ε_2 is noticed to be increased sharply and attains maximum value (5.7) at 8.7 eV frequency. Unfortunately, after that frequency the values of imaginary constant started to decrease and becomes zero at 13 eV frequency.

Refractive index and extinction coefficient

A dimensionless parameter, the refractive index, is in fact a ratio amid velocity of light in a vacuum to the velocity of light passing through the materials. The refractive index, n and dielectric functions (ε_1, ε_2) are interlinked through the following relations [40]:

$\varepsilon_1 = n^2 - k^2(3)\backslash n\varepsilon_2 = 2nk$ (4)

Where k defines the extinction coefficient. Figure 10 displays the material's response associated with refractive index and its imaginary part, i.e., extinction coefficient. The static value of the refractive index n (0) is noted to be 1.5, which however remains unchanged with increasing frequency till 5 eV. Nonetheless, its value grows gradually beyond 5 eV and attains sharp peak at 7.5 eV frequency. Afterwards, the sharp decrease in value of the refractive index has been noticed upto 12.5 eV, which re-escalates at further higher frequency. It has been noticed that refractive index and extinction coefficient both have shown similar pattern as that of the real and imaginary components of the dielectric function. Likewise ε_2, value of the extinction coefficient

remains zero equal to the energy band gap of the considered compound, which is the characteristic of the semiconducting materials [44].

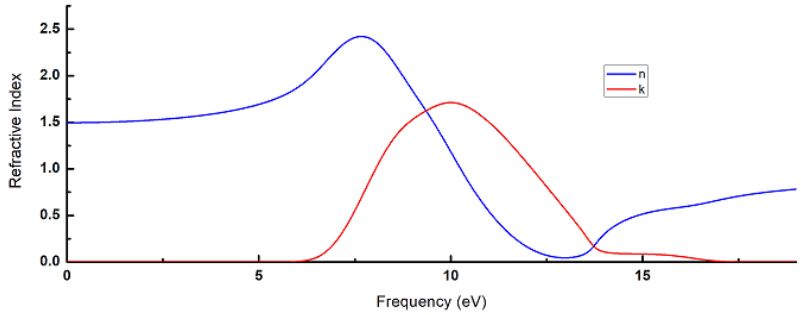

Figure 10: The calculated refractive index (n) and extinction coefficient (k)

Absorption coefficient

The rate of incident electromagnetic radiations rapt in any material can generally be determined through the absorption coefficient, i.e.,$\eta = \frac{2k\omega}{c}$. As shown in Fig. (11), the absorption starts approximately from 6.5 eV frequency because it is prime characteristic of the absorption coefficient that it remains zero upto the energy equal to the energy band gap of any solid material. However, values of the absorption coefficient are found to be increased when incident radiations gain threshold frequency, then it attains its maximum value of 280000 cm^{-1} at 10.25 eV frequency. Rather increasing the absorption rate after this frequency, its values decrease sharply and become zero at 17 eV frequency where incident radiations fall in infrared range of the electromagnetic radiations. Moreover, the absorption coefficient may be associated with band gap energy of a certain material which can further be elaborated in a way that the material having wide band gap could be a best absorber of incident radiations above E_g and vice versa.

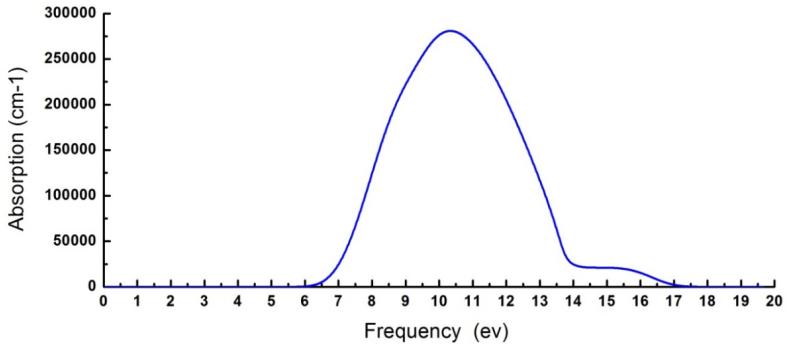

Figure 11: The calculated absorption coefficient.

Optical conductivity

The optical conductivity is displayed schematically in Fig. (12), wherein, blue color line represents real component while red color defines the imaginary part of the conductivity. The real part of the conductivity

is found to be zero till the frequency slightly less than its threshold value. Nevertheless, values of the real conductivity rise abruptly to attain its maximum value of 6.0 $(fs)^{-1}$ at the cut-off frequency of 8.0 eV. Beyond this frequency limit, conductivity decreases sharply, and ultimately becomes zero at 12.5 eV leading to the fact that no incident radiations could pass through the considered compound very far from this particular frequency limit (12.5 eV). Generally, the real part of the optical conductivity has followed the similar fascinating trend as that of the absorption coefficient and imaginary components of the dielectric function/refractive index. As regard the imaginary part of the conductivity has shown counterintuitive behavior since it is found to extend in negative region of the conductivity where maximum conduction of incident electromagnetic radiations has been observed. And that gradual escalation in its values has been noticed, in the region where, real conductivity is being decreased sharply.

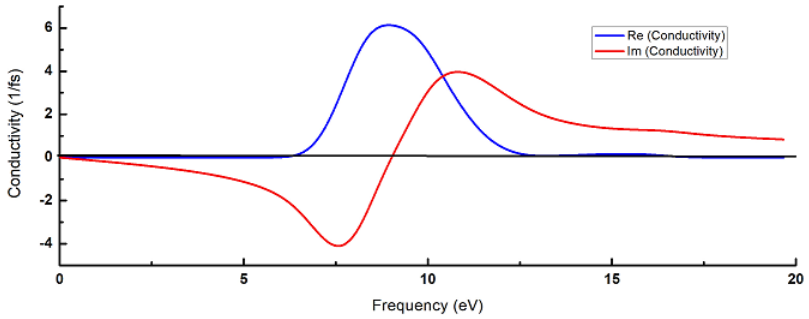

Figure 12: The calculated optical conductivity.

Reflectivity

Portion of the electromagnetic radiations that bounces back from surface of a material can be envisaged by using the reflectivity relation which is expressed as:

$$R\ (\omega)\ =\ \left|\frac{\sqrt{\varepsilon\ (\omega)}\ -1}{\sqrt{\varepsilon\ (\omega)}+1}\right|^2$$

From figure 13, static value of the reflectivity R(0) is 0.05. It increases slowly upto 5 eV, but then upsurges gradually and attains its maximum value of 0.89 at photonic energy of 12.9 eV. It is observed that the reflectivity is maximum in the energy region where absorption was found to reveal decreasing trend.

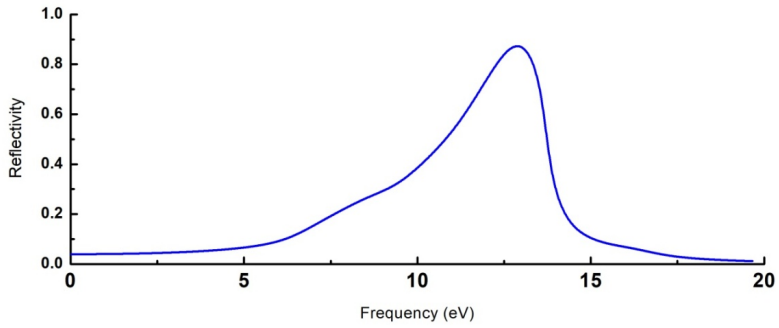

Figure 13: The calculated Reflectivity

Energy Loss Function

Energy loss function determines how much energy is being wasted during motion of fast-moving electrons when they incident upon a material's surface. The frequency at which loss of energy is maximum be recognized as the plasma frequency. Form figure 14, plasma frequency is noted at resonance frequency of 13.7 eV, which indicates that loss function is maximum (with a value of 17) where absorption is found minimum.

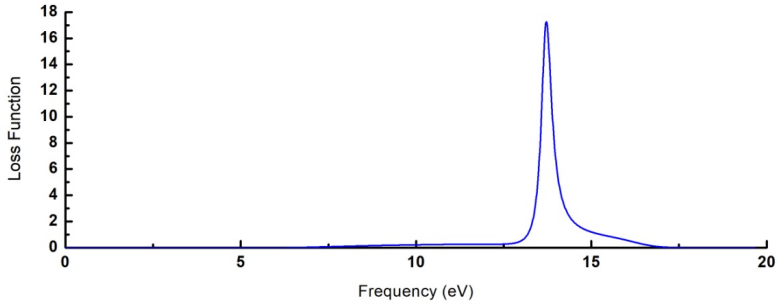

Figure 14: The calculated energy loss function.

Conclusions:

The orthorhombic phase of $LiBH_4$ was found to be suitable for optoelectronic applications. The contributions of Li, B and H atoms are noticed for the modes of vibrations between different range of frequencies, i.e., 0 to 400 cm^{-1}, 1100 to 1300 cm^{-1} and 2250 -2400 cm^{-1}. The low frequency modes between the ranges ˜ 93- 436 cm^{-1} were observed due to displacement of Li^+ and $[BH4]^-$ atoms. The bending modes were noted between the ranges ˜1054-1305 cm^{-1} due to motion of B and H atoms. Moreover, symmetric and antisymmetric stretching modes were found between the frequency values of ˜2303-2401 cm^{-1}due to contribution of H atoms. The calculated values of band gaps of 6.35, 6.81 and 7.58 eV for local, non-local and hybrid functionals indicate that the studied compound is a wide band gap insulator. The mechanical analysis reveals that LiBH4 is a brittle material. Optical analysis also endorsed the value of wide band gap. The plasma frequency is calculated from the highest peak of loss function at energy value of 13.7 eV.

References:

[1] Y. Yurum, A. Taralp, and T. N. Veziroglu, Storage of hydrogen in nanostructured carbon materials, Int. J. Hydrog. Energy. 34 (09) 2009 3784–3798.

[2] R. M. A. Khalil, F. Hussain, A. M. Rana, and M. Imran, Thermodynamics and vibrational study of hydrogenated carbon nanotubes: A DFT study, Phys. B: Physics of Condens. Matt. 530 (2018) 307-311.

[3] P. Jena, Materials for Hydrogen Storage: Past, Present, and Future, J. Phys. Chem. Lett. 02(03) (2011) 206-209.

[4] R. M. A. Khalil, F. Hussain, M. Imran, A. M. Rana, and G. Murtaza, ab-initio study of the exo-hydrogenated single wall carbon nanotubes, Phys. B: Physics of Condens. Matt. 552, (2019) 124-129

[5] H. Wang, Phase transition and electronic properties of $LiBH_4$ via first-principles Calculations, Adv. Mater. Res. 971-973 (2014) 119-122.

[6] M. J. V. Setten, V. A. Popa, G. A. de Wijs, and G. Brocks Electronic structure and optical properties of lightweight metal hydrides, Phys. Rev. B. 75, 035204 (2007).

[7] Mo. Xiaohua, W. Jiang, Dehydrogenation properties of LiBH4 modified by Mg from First-principles calculations, J. Alloys Compd. 735 (2018) 668-676.

[8] K. Miwa, N. Ohba, and Shin-ichi Towata, First-principles study on lithium borohydride LiBH4 Phys. Rev. B 69, 245120 (2004).

[9] T. A. Ikeshoji, E. Tsuchida, T. Morishita, K. Ikeda, M. Matsuo, Y. Kawazoe, S. Orimo, Fast-ionic conductivity of Li+ in $LiBH_4$, Phys. Rev. B 83, 144301 (2011).

[10] Q. Song, Q. Zhao, Z. Jiang, Z. Zhang and Haiyan Zhu, A first-principles Simulation of the metal borohydride ammonia borane complex $(LiBH_4)_2(NH_3BH_3)$ and the decomposition reaction pathway for Hydrogen storage, Int. J. Hydrog. Energy 44 (2019) 20121-20132.

[11] H. Benzidi, M. Garara, M. Lakhal, M. Abdalaoui, A. Benyoussef, A. El kenz, M. Louilidi, M. Hamedoun, O. Mounkachi, Vibrational and thermodynamic properties of $LiBH_4$ polymorphs from first-principles calculations, Int. J. Hydrog. Energy. 43 (2018) 6625-6631.

[12] R.M. A. Khalil, F. Hussain, M. Imran, U. Rasheed, A. M. Rana and G. Murtaza, An *ab-initio* study of spectroscopic and thermodynamic characteristics of MgH_2 and TiC Systems, Int. J. Hydrog. Energy 44 (2019) 6756-6762.

[13] T. Ghellab, Z. Charifi, H. Baaziz, K. Bouferrache and B. Hamad, Electronic structure and optical properties of complex hydrides $LiBH_4$ and $NaAlH_4$ compounds Energy Res. (2018) 1-15.

[14] S. J. Clark, M. D. Segall, C. J. Pickrd, P. J. Haspani, P. J. H. Matt, K. Refson, M. C. Pyne, First principles methods using CASTEP. Z. Kristallogr. Cryst. Mats 220, (2005) 567-570

[15] J. Vackar, M. Hytha, A. Simmunek, All-electron pseudopotentials. Phys Rev B 58, (1998) 12712.

[16] D.H. Hamann, M. Schluter, and C. Chiang, Norm-Conserving Pseudopotentials Phys. Rev 43 (1979) 1494-1497.

[17] D. R. Hamann, Generalized norm-conserving pseudopotentials Phys. Rev. B (1989) 2980.

[18] H. J. Monkhorst and J. D. Pack, Special points for Brillouin-zone integrations, Phys. Rev. B 13, (1976) 5188.

[19] B. G. Pfrommer, M. Cote, S. G. Louie, M. L. Cohen, J. Comput. Phys. 131 (1997) 133.

[20] R.P. Feynman, Forces in Molecules Phys. Rev. 56 (1939) 340.

[21] D.M.Cepreley and B.J.Alder, Ground State of the Electron Gas by a Stochastic Method. Phys. Rev. Lett. 45(7) (1980) 566-569.

[22] J. Heyd, G. E. Scuseria, and M. Ernzerhof, Erratum: Hybrid functionals based on a screened Coulomb potential, J. Chem. Phys. 124, 219906 (2006).

[23] J.P. Pedrew, K. Burke and M. Ernzerhof, Generalized Gradient Approximation Made Simple, Phys Rev Lett 77 (1996) 3865–3868.

[24] P.Hohnberg and W. Kohn, Inhomogeneous Electron Gas, Phys Rev. B 136 (3B) (1964) B864–B871.

[25] W.Kohn and L.J. Sham, Self-Consistent Equations Including Exchange and Correlation Effects, Phys Rev. 140 (4A) (1965) 1133–1138.

[26] X. Gonze, and C. Lee, Dynamical matrices, Born effective charges, dielectric permittivity tensors, and interatomic force constants from density-functional perturbation theory phys. Rev. B 55 (1997) 10355.

[27] Kronig, R.D.L., J. Opt. Soc. Am. On the Theory of Dispersion of X-Rays Phys. Rev. 12 (1926) 547-557.

[28] K. Xiong, J. Robertson, S.J. Clark, Defect states in the high-dielectric-constant gate oxide LaAlO3, Phys. Lett. 89 (2006), 022907.

[29] M. Solar and N. Trapp, A lightweight modular system for handling crystalline samples at low temperatures under inert conditions, J. Appl. Cryst. 51 (2018) 541-548,

[30] S. Baroni , S.d.G., A. dal Corso, P. Giannozzi, Phonons and related crystal properties from density-functional perturbation theory. Rev. Mod. Phys. **73** (2) (2001) 515-562.

[31] K. Miwa, N. Ohba, S. Towata, First-principles study on lithium borohydride $LiBH_4$, Phys. Rev. B 69, 245120 (2004) 1-8.

[32] T. Ghellab, Z. Charifi, H. Baaziz, K. Bouferrache, B. Hamad, Electronic structure and optical properties of complex hydrides $LiBH_4$ and $NaAlH_4$ compounds, Int. J. Energy Res. (2019) 1-15.

[33] Z.J. Wu, E. Zhao, H. P. Xiang, X. F. Hao, X. J. Liu, J. Meng, Crystal structures and elastic properties of superhard IrN_2 and IrN_3 from first principlesPhys. Rev. B 76 (2007) 054115.

[34] D. Mainprice, M. Humbert, Methods of calculating petrophysical properties from lattice preferred orientation data, Surv. Geophys. 15 (1994) 575-592.

[35] M. Hadi, M. Roknuzzaman, A. Chroneos, S. Naqib, A. Islam, R. Vovk, K. Ostrikov, Elastic and thermodynamic properties of new $(Zr_{3-x}Ti_x)AlC_2$ MAX-phase solid solutions, Comput. Mat. Sci. 137 (2017) 318–326.

[36] S. F. Pugh, Relations between the elastic moduli and the plastic properties of polycrystalline pure metals, Philos. Mag. 45 (1954) 823-843.

[37] Y. Tian, B. Xu, Z. Zhao, Microscopic theory of hardness and design of novel superhard crystals, Int. J. Refract. Met. Hard Mater. 33 (2012) 93–106.

[38] I. N. Frantsevich, F. F. Voronov, S. A. Bokuta, Elastic Constants and Elastic Moduli of Metals and Insulators, Handbook Ed. I. N. Frantsevich (Kiev: Naukova Dumka) (1990) 60.

[39] V. Tvergaard, J.W. Hutchinson, Microcracking in ceramics induced by thermal expansion or elastic anisotropy, J. Am. Ceram. Soc. 71 (3) (1988) 157-166.

[40] M. I. Hussain, R. M. A. Khalil, F. Hussain, A. M. Rana, M. Imran, Ab-initio prediction of the mechanical, magnetic and thermoelectric behaviour of perovskite oxides $XGaO_3$ (X = Sc, Ti, Ag) using LDA+U functional: For optoelectronic devices, J. Mol. Graph. Model. 99 (107621) (2020) 1-11.

[41] K. Xiong, J. Robertson, S. J. Clark, Defect States in the High-Dielectric-Constant Gate Oxide $LaAlO_3$ Appl. Phys. Lett. 89(2) (2006).

[42] P. Baroni and S. Picozzi, Mechanisms and origin of multiferroicity. C. R. Physique 16 (2015) 143-152

[43] D. R. Penn, Wave-Number-Dependent Dielectric Function of Semiconductors, Phys. Rev. 128 (1962)2093-2097

[44] M. I. Hussain, R. M. A. Khalil, F. Hussain, M. Imran, A. M. Rana, S. Kim, Investigations of structural, electronic and optical properties of $YInO_3$ (Y = Rb, Cs, Fr) perovskite oxides using mBJ approximation for optoelectronic applications: A first principles study. Mater. Sci. Semicond. Process. 113, (2020) 1-9.

[45] S. Gomes, H. Hagemann, K. Yvon, Lithium boro-hydride $LiBH_4$: II. Raman spectroscopy, J. Alloys Compd. 346 (2002) 206–210.